A Non-Innocent Coordination Chemistry Approach to 2D Conductive Magnets

Kasper S. Pedersen[1,2,3]*, Panagiota Perlepe[1,2,4,5], Michael L. Aubrey[6], Daniel N. Woodruff[7], Sebastian E. Reyes-Lillo[8,9], Anders Reinholdt[10], Mathieu Rouzieres[1,2], Dumitru Samohvalov[1,2], Fabrice Wilhelm[11], Andrei Rogalev[11], Jeffrey B. Neaton[8,12], Jeffrey R. Long[6,13,14] and Rodolphe Clérac[1,2]*

The unique properties of graphene, molybdenum disulfide, and other 2D materials have boosted interest in layered metal-organic coordination solids, sometimes referred to as metal-organic graphene analogues. In particular, achieving 2D materials, that behave as both conductors and magnets, paves the way towards applications in quantum magnetoelectronics and spintronics. Reaction of $CrCl_2$ with pyrazine (pyz) affords $CrCl_2(pyz)_2$, a pyrazine-bridged, layered coordination solid. This air-stable compound displays a ferrimagnetic order below ~55 K, reflecting the presence of a strong magnetic communication between spin-carriers. X-ray spectroscopy results indicate the presence of Cr(III) centers with a significantly reduced magnetic moment. These properties are induced by the redox non-innocence of the pyrazine ligand, which leads to a smearing of the Cr 3d and pyrazine π states. Electrical conductivity measurements demonstrate $CrCl_2(pyz)_2$ to reach a conductivity of 32 mS cm^{-1} at room temperature and to operate via a 2D hopping-based transport mechanism. This chemical approach, benefitting from ligand non-innocence in conjunction with reducing nature of the paramagnetic metal centers, offers a new appealing strategy to design synthetically tunable 2D materials in which magnetism and electronic conductivity coexist.

Two-dimensional (2D) materials offer a plethora of extraordinary properties not seen in 3D materials, that are central to emergent molecular-scale electronics[1]. However, existing 2D materials such as atomic-thickness layers or hetero-structures of graphene[2] and transition metal disulfides,[3] have limitations and their exceedingly simple chemical nature leaves only little possibility to modulate their electronic, magnetic or optical properties for specific applications. Furthermore, almost all these 2D materials are inherently nonmagnetic,[4] hampering their use in emerging technologies taking advantage of the quantum spin of the transported electrons as spintronics[5], magnetoelectrics[6], and multiferroics[7]. In contrast, transition metal-doped semiconductors are of particular interest for spintronics application due to their near-total spin polarization[8,9]. However, the precise distribution of metal ions is difficult to control and spatially low-dimensional systems have not been obtained. For molecule-based systems, significant efforts have been devoted to improving and tailoring the characteristics of magnets[10] and conductors[11], and a combination of these properties is typically only found in materials having separate magnetic and conductive sublattices[12,13].

An alternative approach to 2D materials is inspired by reticular molecule-based metal-organic framework (MOF) chemistry[14]. The synthetic engineering of the inorganic and organic modules leads to almost endless possibilities for tuning both the physical properties and the anisotropy of the chemical bonding in a 3D crystalline solid. Interestingly, recent reports have shown great promises for the isolation of novel 2D materials as single sheets or van der Waals heterostructures through exfoliation of coordination solids featuring weak dispersion forces between covalently bonded layers[15]. In order to introduce strong electronic and magnetic communication between spin-carriers in such coordination solids, extensive electronic delocalization is essential[16]. Indeed, record high electronic conductivities have been obtained in 2D coordination polymers of ditopic or polytopic conjugated organic ligands and transition metal ions, owing to strong π-d conjugation between the ligand and metal ion orbitals[17,18,19,20,21,22]. However, all of these materials are non-magnetic and involve only square-planar coordinated metal ions. To expand the perspective to the ubiquitous octahedrally coordinated metal ions, recent attention was turned towards multidimensional coordination networks involving Fe[II/III]-benzoquinone radical units[23,24]. However, restraining the chemistry to only those (and a few related) redox partners puts significant limitations on the materials that can be exploited. Indeed, many other metal ion-ligand couples are known to exhibit interesting inner-sphere redox reactions. For instance, several aromatic amines are known to be redox-"non-innocent"[25] when coordinated to moderately reducing transition metal ion centres, often resulting in remarkable electronic structures and reactivities for the molecular species[26]. In an attempt to
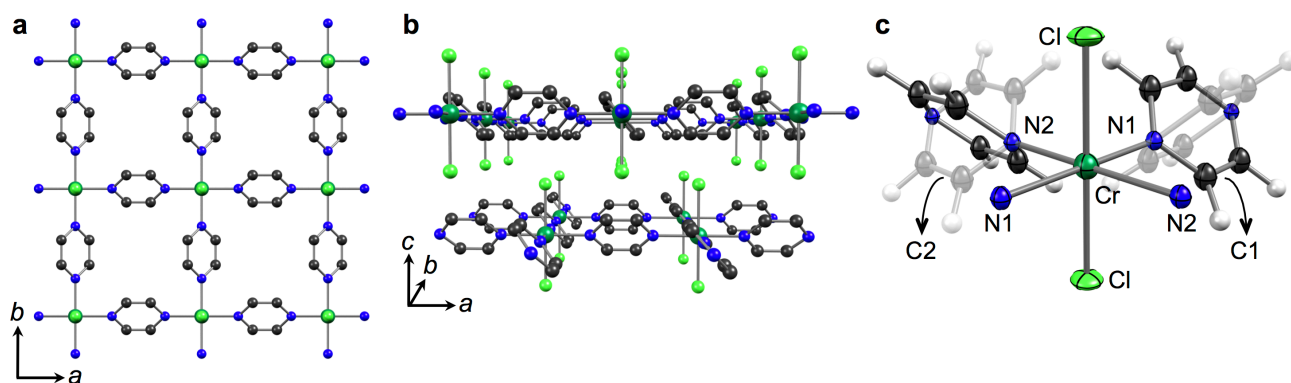
Figure 1 | Structure of CrCl₂(pyz)₂. a, a fragment of the layered structure shown along the Cl–Cr–Cl axis (crystallographic *c* direction), as determined from synchrotron X-ray powder diffraction data at room temperature. **b**, perspective view of the staggered stacking of the layers perpendicular to the *c* direction. **c**, thermal ellipsoid plot drawn at 80% probability level showing the positional disorder of the pyrazine rings. Color code: dark green, Cr; light green, Cl; blue, N; dark grey, C. For the matter of clarity, hydrogen atoms have been omitted in **a** and **b**. Selected bond lengths (Å) and angles (°): Cr–N1 2.003(2), Cr–N2 2.059(2), Cr–Cl 2.337(1), N1–C1 1.349(2), C1–C1 1.327(3), N2–C2 1.333(2), C2–C2 1.351(3), ∠dihedral C1–N1–Cr–Cl 42.5, ∠dihedral C2–N2–Cr–Cl 43.9.

extend this chemistry to coordination networks and to boost both magnetism and electronic conductivity in related 2D materials, we turned our attention to the possible redox non-innocence of the simple pyrazine (pyz) ligand. This common ditopic ligand in chemistry is found in thousands of crystallographically characterized coordination networks [27]. Whilst the pyrazine anion radical can be generated by alkali metal reduction in solution [28] or recently by photon-assisted charge-separation in the solid phase [29], the first indication of a transition metal ion reduction of pyrazine was reported in 1980 by Dunne and Hurst [30]. The purported $[Cr^{III}(Hpyz^{\bullet})]^{3+}$ complex, called "pyrazine green" [31], formed from the reaction between Cr^{2+} and pyrazine in aqueous solution was shown to decay quickly to form $[Cr^{III}(pyz)]^{3+}$ and the dihydropyrazinium radical ion $H_2pyz^{\bullet+}$. Inspired by these results, we report the isolation and characterization of a structurally simplistic 2D coordination solid, **CrCl₂(pyz)₂**, which represents an exceedingly rare example of a molecule-based material showing both long-range magnetic order and high electronic conductivity.

Results and discussion

The reaction of CrCl₂ with a large excess of pyrazine at 200 °C affords a black microcrystalline powder. The elemental analysis of Cr, Cl, N, C, and H, is consistent with the CrCl₂(pyz)₂ formulation (cf. Methods). The crystal structure, shown in Figure 1, was solved from synchrotron X-ray powder diffraction data (cf. Methods, Figure S1). **CrCl₂(pyz)₂** crystallizes as a layered structure in the orthorhombic *Immm* space group. The *trans*-CrCl₂(pyz)₂ layers are stacked along the crystallographic *c* direction and spaced apart by 5.4 Å. Without indications of a larger supercell from the analysis of the powder diffraction pattern, the pyz rings are disordered on two positions imposed by the mirror planes of the *Immm* space group (Figure 1c). Despite the orthorhombic space group, the 2D network closely approaches the symmetry of a square lattice with Cr···Cr distances of 6.90351(4) and 6.97713(4) Å and Cr–N bond lengths of 2.003(2) and 2.059(2) Å (Figure 1, caption). Interestingly, the Cr–Cl bond length (2.337(1) Å) is much shorter than the 2.80 Å found in the related, mononuclear complex *trans*-[Cr^{II}Cl₂(pyridine)₄] [32]. Indeed, the metric parameters of the Cr site in **CrCl₂(pyz)₂** are in the

expected range for Cr^{3+}, as illustrated by *trans*-[CrCl₂(pyridine)₄](ClO₄)·1/4H₂O (**Cr(III)**) having Cr–N and Cr–Cl bond lengths of 2.1 Å and 2.3 Å, respectively.

Since examples of apparent absence of a Jahn-Teller axis in Cr^{2+} complexes have been reported [33], further insight into the Cr oxidation state in **CrCl₂(pyz)₂** was obtained using X-ray absorption spectroscopy (XAS). XAS spectra were collected at the Cr K-edge of **CrCl₂(pyz)₂**, and two mononuclear model complexes (**Cr(II)** and **Cr(III)**, cf. Figure 2, caption), both featuring a {CrN₄Cl₂} chromophore but possessing established +II and +III oxidation states, respectively. The experimental spectra shown in Figures 2a and S3a are dominated by the 1s → 4p transitions with much weaker pre-edge, dipole forbidden, 1s → 3d transitions. The rising edge commences at lower photon energy for **Cr(II)** than for **Cr(III)**, reflecting the stronger binding energy of the 1s core electrons in the latter. As discussed by Wieghardt and coworkers [34], the energetically lowest-lying pre-edge
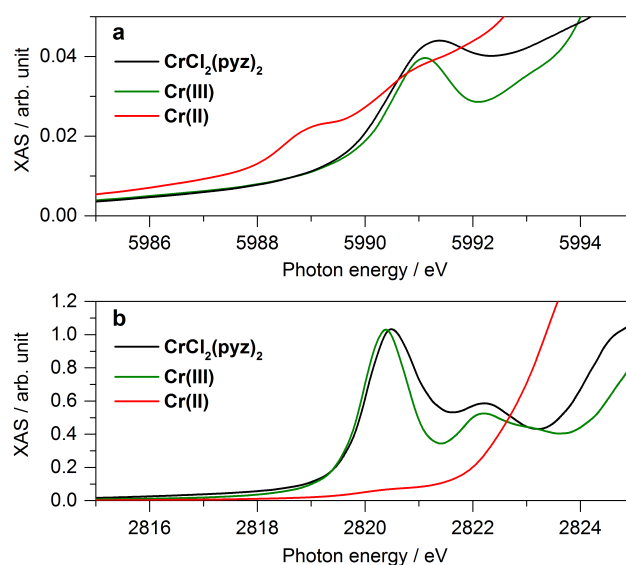
Figure 2 | X-ray absorption spectroscopy (XAS) at the pre-K-edge region. a, Cr K-edge spectra of **CrCl₂(pyz)₂**, **Cr(III)** (*trans*-[Cr^{III}Cl₂(pyridine)₄](ClO₄)·1/4H₂O), and **Cr(II)** (*trans*-[Cr^{II}Cl₂(NCNH₂)₄]) recorded at *T* = 3 K. **b**, Cl K-edge spectra of the same compounds. To facilitate a direct comparison, the data were normalized to zero before the edge and to unity far above the edge (Figure S3).
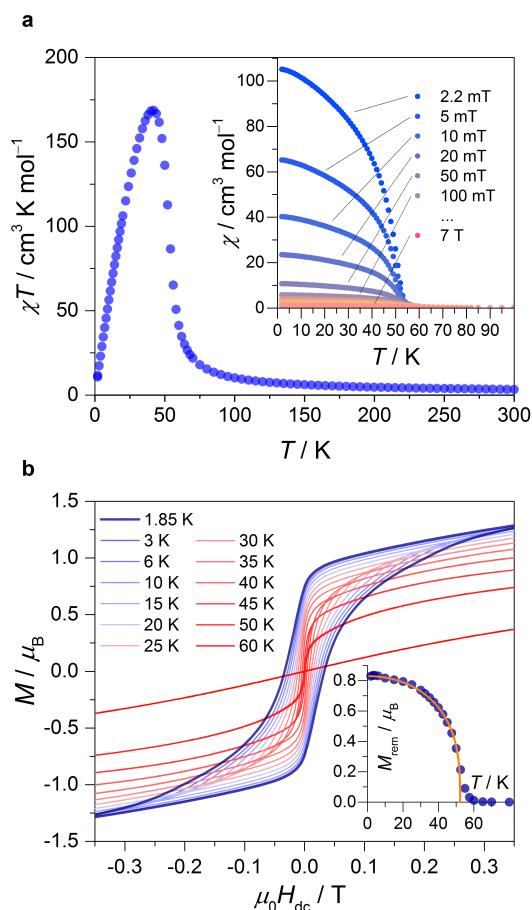
Figure 3 | Magnetic properties for CrCl₂(pyz)₂. **a**, temperature dependence of the χT product ($\mu_0 H_{dc}$ = 0.1 T). Inset: Temperature dependence of the susceptibility at selected dc magnetic fields. **b**, magnetic field dependence of the magnetization obtained with a sweep rate of 30 Oe min⁻¹. The inset shows the temperature dependence of the remnant magnetization deduced from Figure 3b. The solid line is a simulation of the temperature dependence of the remnant magnetization, $M_{rem} \propto (1 - (T/T_c)^\alpha)^\beta$ with T_c = 52 K and β = 0.33.

feature, 1s → t₂g, is a fingerprint of the Cr oxidation state, which is largely insensitive to the exact ligand field. The comparison of the Cr K-edge XAS spectra reveals a remarkable overlap of the **CrCl₂(pyz)₂** and **Cr(III)** data (Figure S3a) with an energy of the pre-edge feature for **CrCl₂(pyz)₂** that is only 0.2 eV higher than that of **Cr(III)** (Figure 2a) The X-ray crystallographic and spectroscopic analyses therefore both point towards the presence of Cr³⁺ in **CrCl₂(pyz)₂**, which necessitates that the pyz scaffold has been reduced by one electron per formula unit during the synthesis. The Cl K-pre-edge intensity provides direct access to the Cl 3p character in the Cr d-orbitals and thus serves as a complementary probe of the Cr electronic structure[35]. The Cl K-edge spectra of **CrCl₂(pyz)₂** and **Cr(III)** are strikingly similar (Figures 2b and S3b), whereas the pre-edge intensity for **Cr(II)** is significantly much lower. These XAS data thus corroborate unequivocally the similar Cr electronic structure in **CrCl₂(pyz)₂** and the archetypal Cr³⁺ complex, **Cr(III)**.

The susceptibility-temperature product, χT, of **CrCl₂(pyz)₂** which amounts to 3.3 cm³ K mol⁻¹ at 300 K (Figure 3), significantly increases when decreasing the temperature. This thermal behavior at high temperatures highlights the presence of remarkably strong magnetic interactions between spin carriers. The direct comparison

of the χT product at 300 K with the Curie constant values (1.9 cm³ K mol⁻¹ for $S = 3/2$ Cr³⁺; 3.0 or 1.0 cm³ K mol⁻¹ for $S = 2$ high-spin or $S = 1$ low-spin Cr²⁺, respectively; 2.25 cm³ K mol⁻¹ for uncoupled $S = 3/2$ Cr³⁺ and $S = ½$ pyrazine radical spins; with $g = 2$) is thus not straightforward. These magnetic susceptibility data are also poorly described by the Curie-Weiss law, as expected for low dimensional systems showing strong π-d conjugation and strong magnetic interactions[36]. A sudden increase of the susceptibility is observed at ~55 K, suggesting the existence of a magnetic phase transition (Figures 3, inset, and S4). This result is corroborated by alternating current (ac) susceptibility data (Figure S5), which show an abrupt increase in both the in-phase (χ') and the out-of-phase (χ'') susceptibilities at ~55 K. The field dependence of the magnetization shows a hysteretic behavior with a remnant magnetization below ~55 K (Figures 3, inset, and S6), further supporting the assignment of an ordering transition at ~55 K. Notably, this ordering temperature is much higher than observed for any previously reported pyrazine-based networks. The saturation magnetization at 7 T and 1.85 K amounts to 1.8 μ_B, which is much lower than expected for a ferromagnetically coupled Cr³⁺-radical pair (~4 μ_B) but that is close to the ~2 μ_B expected for antiferromagnetically coupled Cr³⁺-radical spins. This result supports unambiguously the existence of a ordered ferrimagnetic (FI) state below 55 K with large antiferromagnetic (AF) interactions within the 2D coordination network and an effective inter-layer ferromagnetic coupling.

DFT calculations performed on the simple model fragment, *trans*-[CrCl₂(pyz)₄], reveal significant spin density on the dangling pyrazines (Figure S7), and a broken-symmetry calculation provides a rough estimate for the extremely strong AF Cr³⁺–pyz radical exchange coupling around of –2000 cm⁻¹ (J/hc = –2040 cm⁻¹ with the –2J convention). The calculated Mulliken spin-densities of the $S = 3/2 - S' = 1/2$ broken-symmetry state are given in Figure 4a. The summed spin-density of the pyz ligands of –0.68 μ_B is close to the idealized value for a one-electron reduced array. In order to further elucidate the electronic and magnetic ground state of **CrCl₂(pyz)₂**, periodic lattice
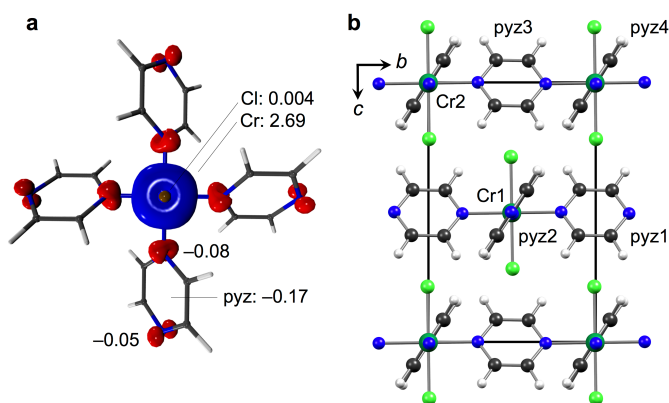

Figure 4 | Density functional theory calculations. **a**, DFT-calculated spin-density (in μ_B) of the broken-symmetry state of the hypothetical [CrCl₂(pyz)₄] model complex in gas phase (isosurface value ±0.005). **b**, DFT-relaxed structure of **CrCl₂(pyz)₂** with fixed experimental lattice constants. The labeling highlights structurally distinct units. Calculated spin moments in units of μ_B for the FI (AF) state: Cr1 2.54 (–2.54), pyz1 –0.32 (0.31), pyz2 –0.28 (0.28), Cr2 2.54 (2.54), pyz3 –0.26 (–0.26), pyz4 –0.27 (–0.26). The local N and C magnetic moments were –0.12 (0.008) and –0.011 (0.001), respectively, and the Cl moments are negligibly small.

DFT calculations were performed on the experimentally observed FI state and on the likely low-lying AF ordered phase (see Methods). Whilst both configurations feature AF interactions within the layers, the difference arises from the nature of interactions between the layers. The DFT optimized structures with fixed experimental lattice constants are similar for both the FI and AF states and close to the experimentally determined structure. The optimized C–N–Cr–Cl torsion angles are in the 33–36° range leading to pyrazine rings, which are slightly less tilted than in the experimental structure (43–44°). In both cases, an absolute local magnetic moment of ~2.4 μ_B is found for each Cr^{3+} ion (Cr1 and Cr2 in Figure 4b), which is significantly reduced from the expected ~3 μ_B for Cr^{3+}. As expected, the local magnetic moments of the pyrazine ligands (pyz$x$, x = 1–4, Figure 4b) are always antiparallel to the nearest Cr moment. Remarkably, the resulting magnetization at saturation for the 2D network is estimated as 1.8 μ_B, in perfect agreement with the experiment (Figure S6). Thus, the difference between the possible FI and AF ordered states arise only from the respective orientation (parallel versus antiparallel, respectively) of the $CrCl_2(pyz)_2$ layer magnetic moments (cf. Figure 4, caption). Interestingly, these FI and AF states are virtually degenerate at this level of theory (within ~10 cm^{-1} per formula unit), highlighting the very weak interlayer magnetic interactions as compared to the intralayer ones.

In an attempt to determine experimentally the magnitude of the local Cr moment in $CrCl_2(pyz)_2$, X-ray magnetic circular dichroism (XMCD) experiments were performed. At the Cr K-edge, the XMCD signal is due to the orbital polarization of the Cr 4p- and 3d-states that could be induced either by the intra-atomic spin-orbit interaction of the Cr atoms and (or) by hybridization of the Cr 4p-states with spin–orbit split states of neighboring atoms [37]. Given the fact that spin-orbit interactions of the pyz ligand atoms are negligibly small, the second term can be simply neglected. Thus, the observed XMCD signals at the Cr K-edge are due to Cr magnetization only, and their intensity is directly proportional to the magnetic moment of the absorbing atom. The XMCD spectra of $CrCl_2(pyz)_2$ and Cr(III) shown in Figure 5 reveal several clear features in the pre-edge († in Figure 5), at the edge (‡) and also characteristic super-Coster-Kronig multi-electron excitations (§)[38]. The pre-edge signal originates from electric quadrupolar

transitions in Cr ions (1s → 3d) while the negative XMCD peak at the edge involves the 4p states which are polarized by the 3d states. The multi-electron excitations involve also transitions from shallow core 3p states into 3d states and could be also considered as a fingerprint of 3d moment. Remarkably, the XMCD spectra of Cr(III) and $CrCl_2(pyz)_2$ have basically the same shape including multielectron excitations, that confirms the identical local electronic structure of Cr ions in these systems. Indeed, the intensity of XMCD spectrum of Cr(III) can be scaled by 0.75 factor to the $CrCl_2(pyz)_2$ spectra to yield an essentially perfect overlap. Considering the bulk magnetization of the Cr(III) model complex (Figure S8) which saturates at 3.1 μ_B, the local Cr magnetic moment in $CrCl_2(pyz)_2$ can thus be estimated at 2.3 μ_B. Notably, the Cr moment is strongly reduced from the expected ~3 μ_B, as already concluded from the DFT calculations (2.4 μ_B, *vide supra*) and in excellent agreement with the low experimental value of the $CrCl_2(pyz)_2$ magnetization at saturation.

Organic mixed-valence systems with strong through-metal coupling were recently reported by some of us as a convenient design principle to yield new conductive MOFs[23]. Likewise, it is straightforward to imagine the highly delocalized open shell frontier states of $CrCl_2(pyz)_2$ could also allow for bulk electronic conductivity. The black color of $CrCl_2(pyz)_2$ was a promising indicator of indispensable low-energy electronic excitations, which are clearly detected by UV-vis-NIR diffuse reflectance spectroscopy (Figure 6, inset) with a strong, very broad, absorption band that is steadily increasing in intensity from 6 down to 0.5 eV. These strong absorption features extend into the MIR region (Figure S9), suggesting a quasi-continuous distribution of localized mid-gap states in close energetic proximity[39,40]. The temperature dependence of the electrical conductivity, σ, of $CrCl_2(pyz)_2$ is shown in Figure 6a. The room temperature conductivity amounts to σ_{RT} = 32 mS cm^{-1}, which places $CrCl_2(pyz)_2$ amongst the more conducting

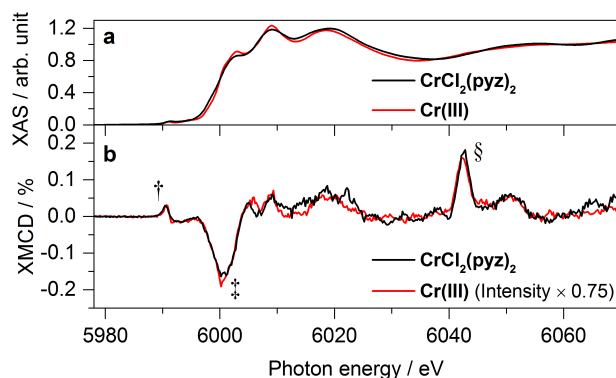**Figure 5 | X-ray magnetic circular dichroism (XMCD). a**, normalized XAS spectra of $CrCl_2(pyz)_2$ and Cr(III); **b**, corresponding XMCD spectra. These data were obtained at 3 K with a magnetic field of 17 T. The labeled spectral features correspond to pre-edge (†), edge (‡), and multi-electron excitations (§).
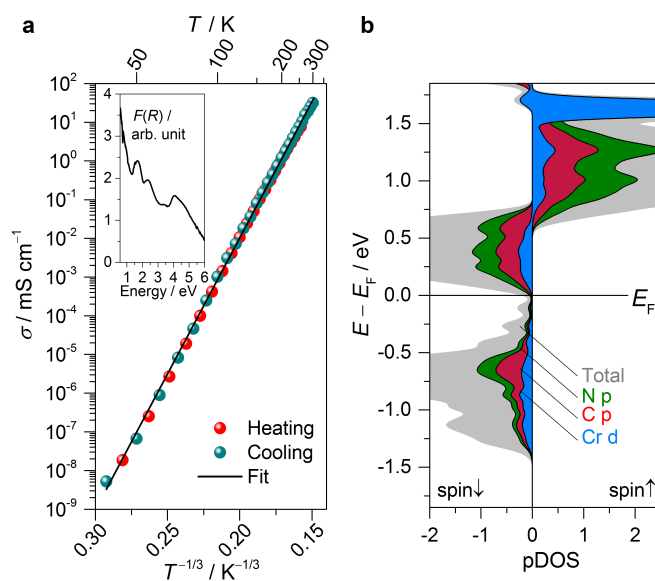

Figure 6 | Electrical conductivity. a, temperature dependence of the 2-contact conductivity of $CrCl_2(pyz)_2$. The solid line is the best fit to the 2D-Mott law described in the Methods with σ_0 = 1.2 × 10^{12} mS cm^{-1} and T_0 = 4.2 × 10^6 K. The inset shows the Kubelka-Munk transformation of the room temperature diffuse reflectance spectrum of $CrCl_2(pyz)_2$. **b**, first-principles projected density of states (pDOS) of the FI state of $CrCl_2(pyz)_2$, showing the major contributions of the N p and C p states to the conduction band.

coordination solids reported so far[16,17]. In contrast to, for example, organic-based charge-transfer salts[11,41], the lack of π-π interactions in **CrCl₂(pyz)₂** suggests the presence of a transport mechanism involving both ligand π-orbital and metal d-orbitals. The soft exponential decrease of the conductivity with decreasing temperature suggests an insulating ground state for **CrCl₂(pyz)₂** with a charge transport dominated by a thermally activated hopping mechanism. Indeed, the temperature dependence of σ could be modeled well by the 2D-Mott law invoking a variable-range hopping mechanism (see Methods) commonly used to describe bulk transport of Mott-Hubbard insulators (Figure 6)[42]. The DFT calculations predict metallic and insulating ground state for the FI and AF phases, respectively with direct and indirect band gaps given by 0.42 and 0.19 eV at Γ and close to Γ (Figure S10). While absorption spectroscopy agrees with a small optical band gap, conductivity measurements do not support a metallic ground state (cf. the projected density of states, pDOS, Figure 6b). Most likely, this discrepancy between theory and experiments might found its origin in the structural disorder of the pyrazine ligands which is not captured in the extended structure DFT calculation. In low dimensional solids, charge localization is commonly induced by disorder that is difficult to account for in a perfect crystal calculation. The pDOS (Figure 6b) also supports the potential impact of the pyrazine disorder on the conductivity properties of **CrCl₂(pyz)₂** as the frontier orbitals of the valence and conduction bands are dominated by organic C and N 2p states. On the other hand, the contributions from the Cr d states are somewhat smaller and become only dominant from ~1.5 eV above the Fermi level. Notably, the Cr d states show significant dispersion, which further supports a strong π-d hybridization[43].

Outlook

In this report, we have shown how the redox non-innocence of a simple ligand like pyrazine can be employed to enhance the electronic and magnetic communication in 2D molecule-based materials exemplified by the coordination solid, **CrCl₂(pyz)₂**. Whilst structural and X-ray spectroscopic data point toward an oxidation state assignment of +III for the Cr site, its magnetic moment is significantly lower than the expected Cr³⁺ value. DFT calculations suggest a strong degree of π-d conjugation, which, to a certain extent, washes out the concept of a metal ion oxidation state, but provides a high magnetic ordering temperature and a remarkably large electronic conductivity. In that sense, **CrCl₂(pyz)₂** can be considered as a 2D version of the numerous molecular (0D) complexes based on low-valent metal ion, which have shown strong ligand non-innocence and fascinating electronic structures[44]. Likewise, it can envisioned that 2D coordination solids with improved properties can be designed using strongly reducing transition metal ions in conjunction with organic ligands previously considered to be wholly innocent. Additionally, it should be stressed that **CrCl₂(pyz)₂** shows an attractive resemblance to the cuprates in terms of symmetry, magnetic exchange interactions,[45] and π-d conjugation[46]. These results therefore open up exciting new synthetic prospects for novel magnetic conductors derived from metal-organic coordination solids and capable of generating spin-polarized currents in low-dimensional devices.

Methods

Synthesis. All handling of **CrCl₂(pyz)₂** was performed under a dry N₂ or Ar atmosphere. A 50-mL Teflon-lined stainless steel autoclave reactor was charged with CrCl₂ (0.20 g, 3.8 mmol; Aldrich, 99.99% trace metal basis) and pyrazine (2.0 g, 25 mmol; Aldrich, ≥99%) and placed in an oven (200 °C) for 24 h. The reactor was cooled to room temperature and the purple-black microcrystalline product of **CrCl₂(pyz)₂** was washed with a 20-mL aliquot of *N,N*-dimethylformamide and 2 × 20-mL of acetonitrile and dried *in vacuo*. Yield: 70-75% Elemental analyses were performed at the Mikrolab Kolbe (Mülheim an der Ruhr, Germany). Anal. Calcd. (found) for C₈H₈Cl₂CrN₄, Cr: 18.37% (18.12%), Cl: 25.05% (25.33%), C: 33.94% (33.96%), H: 2.85% (2.94%), N: 19.79% (19.57%). Sum: 100% (99.92%). The IR spectrum is largely uninformative due to strong absorption as described in the main text. Characteristic Raman (Horiba Scientific XploRA, λ_{inc} = 785 nm) shifts (cm⁻¹): 670, 1029, 1221, 1613. UV-visible-NIR diffuse reflectance spectra were collected using a CARY 5000 spectrophotometer interfaced with Varian Win UV software. The samples were held in a Praying Mantis air-free diffuse reflectance cell. Polyvinylidene fluoride (PVDF) powder was used as a non-adsorbing matrix.

X-ray Spectroscopy. XAS and XMCD spectra were obtained at the ID12 beamline (ESRF – The European Synchrotron). We used fundamental harmonic of Apple-II type undulator for experiments at the Cr K-edge, whereas Cl K-edge data were collected using the fundamental harmonic of Helios-II type undulator. All XAS spectra were recorded using total fluorescence yield detection mode and were subsequently corrected for reabsorption effects. The XMCD spectra were obtained as the difference between two consecutive XAS spectra recorded with opposite photon helicities. Furthermore, the XMCD spectra were systematically obtained in both magnetic field directions (at 17 T) in order to ensure the absence of experimental artifacts.

DFT calculations. Periodic lattice DFT calculations were performed with VASP[47,48]. We use the Heyd-Scuseria-Ernzerhof (HSE) hybrid functional[49], where 25% of the generalized gradient approximation[50] exchange is replaced with exact Hartree-Fock exchange, and the long-range interaction is screened with a range separation parameter of 0.2 Å⁻¹. Our calculations use a plane-wave energy cut-off of 450 eV, a 4 × 4 × 2 Γ centered k-point grid, and projected augmented pseudo-potentials with 14, 7, 4, 5 and 1 valence electrons for Cr, Cl, C, N, and H, respectively, from the VASP library[51]. Projected density of states (pDOS) are computed using a denser 6 × 6 × 4 Γ centered k-point grid. Convergence studies show that band gaps are converged within 0.01 eV using a cut-off energy of 450 eV. In order to account for the quasi-random orientation of the pyrazine rings, we simulated the room temperature structure of **CrCl₂(pyz)₂** by considering different relative orientations of the four pyrazine rings in the two-formula unit supercell structure. Structural relaxations were performed using the HSE functional until atomic forces were smaller than 0.1 eV Å⁻¹. We note that full relaxation of the structure yields an unphysical distortion due to its two-dimensional nature, and we therefore fixed the lattice constants to the experimental values.

Electrical conductivity. The two-contact variable temperature conductivity was conducted in a home built two-electrode screw cell with a contact area of 0.04757 cm². In an argon-filled glove box, pellets were pressed between two copper rods with contacts polished to a mirror finish. The screw cell was sealed with Torr Seal® low vapor pressure epoxy to make an airtight seal. Two-contact conductivity measurements were performed in a Quantum Design MPMS2 SQUID magnetometer with a dc-transport rod modified to accommodate two 26 AWG silver coated copper cables sealed at the top of the rod with a gas tight Swagelok fitting and Torr Seal® low vapor pressure epoxy. The sample cell was attached to the rod and descended into the cryostat-equipped SQUID chamber. *I-V* profiles were collected with a Bio-Logic SP200 potentiostat with 30 nA current resolution. All data collected were Ohmic within a ±1 V window with a very small apparent temperature hysteresis that vanished after thermal cycling and equilibration at 300 K. The resulting *I-V* profiles were modeled with Ohm's law, $E \times \sigma = j$, where E is the applied electric field and j is the current density, to determine the sample conductivity, σ, with units of Ω^{-1} cm^{-1}. The temperature dependence of conductivity was fit to the Mott law relevant for a variable-range hopping mechanism:

$$\sigma(T) = \sigma_0 \exp\left(-\frac{T_0}{T}\right)^{\frac{1}{d+1}} \qquad (1).$$

Here, d is the dimensionality of transport (in the present case of a 2D lattice, $d = 2$), and σ_0 and T_0 (Mott temperature) are empirical constants related to the carrier density and localization length of the hopping electron.

Further synthetic, characterization, magnetic, crystallographic and computational details are described in the Supplementary Methods.

Acknowledgements

Author contributions

K.S.P. and R.C. conceived, planned, and designed the research project. K.S.P., P.P., D.W., A.R. and D.S. executed the syntheses and the chemical and crystallographic analyses. M.L.A., M.R., P.P., J.R.L. and R.C. performed and analyzed the electrical conductivity experiments. M.R., K.S.P. and R.C. performed and analyzed the magnetic susceptibility measurements. S.E.R.-L., J.N. and K.S.P. performed the DFT studies. F.W., A.R., K.S.P., P.P. and R.C. executed the X-ray spectroscopy experiments and analyzed the results. All coauthors were involved in the writing of the manuscript and they have all given their consent to its publication.

Additional information

Reference

1. Novoselov, K. S., Mishchenko, A., Carvalho, A. & Castro Neto, A. H. 2D materials and van der Waals heterostructures. *Science* **353**, aac9439, (2016).
2. Novoselov K. S. *et al.* Electric Field Effect in Atomically Thin Carbon Films. *Science* **306**, 666–669 (2004).
3. Chhowalla, M. *et al.* The chemistry of two-dimensional layered transition metal dichalcogenide nanosheets. *Nat. Chem.* **5**, 263–275 (2013).
4. Huang, B. *et al.* Layer-dependent ferromagnetism in a van der Waals crystals down to the monolayer limit. *Nature* **546**, 270–273 (2017).
5. Han, W., Kawakami, R. K., Gmitra, M. & Fabian, J. Graphene spintronics. *Nat. Nanotech.* **9**, 794–807 (2014).
6. Tian, Y. *et al.* Observation of Resonant Quantum Magnetoelectric Effect in a Multiferroic Metal–Organic Framework. *J. Am. Chem. Soc.* **138**, 782–785 (2016).
7. Gómez-Aguirre, L. C. *et al.* Magnetic Ordering-Induced Multiferroic Behavior in [CH$_3$NH$_3$][Co(HCOO)$_3$] Metal-Organic Framework. *J. Am. Chem. Soc.* **138**, 1122–1125 (2016).
8. Dietl, T., Ohni, H., Matsukura, F., Cibert, J. & Ferrand, D. Zener model description of ferromagnetism in zinc-blende magnetic semiconductors. *Science* **287**, 1019–1022 (2000).
9. Yu, J. H. *et al.* Giant Zeeman splitting in nucleation-controlled doped CdSe:Mn^{2+} quantum nanoribbons. *Nat. Mater.* **9**, 47–53 (2010).
10. Miller, J. S. Magnetically ordered molecule-based materials. *Chem. Soc. Rev.* **40**, 3266–3296 (2011).
11. Batail, P. (Ed.) Molecular Conductors. *Chem. Rev.* **104**, 4887–5782 (2004).
12. Coronado, E. Galán-Mascarós, J. R., Gómez-García, C. J. & Laukhin, V. Coexistence of ferromagnetism and metallic conductivity in a molecule-based layered compound. *Nature* **408**, 447–449 (2000).
13. Coronado, E. & Day, P. Magnetic Molecular Conductors. *Chem. Rev.* **104**, 5419–5448 (2004).
14. Yaghi, O. M. *et al.* Reticular synthesis and the design of new materials, *Nature* **423**, 705–714 (2003).

15. Hermosa, C. *et al.* Mechanical and optical properties of ultralarge flakes of a metal–organic framework with molecular thickness. *Chem. Sci.* **6**, 2553–2558 (2015).

16. Givaja, G., Amo-Ochoa, P., Gómez-García, C. J. & Zamora, F. Electrical conductive coordination polymers. *Chem. Soc. Rev.* **41**, 115–147 (2012).

17. Sun, L., Campbell, M. G., & Dincǎ, M. Electrically Conductive Porous Metal–Organic Frameworks. *Angew. Chem. Int. Ed.* **55**, 3566–3579 (2016).

18. Kambe, T. *et al.* π-Conjugated nickel bis(dithiolene) complex nanosheet. *J. Am. Chem. Soc.* **135**, 2462–2465 (2013).

19. Sheberla, D. *et al.* High Electrical Conductivity in $Ni_3(2,3,6,7,10,11$-hexaiminotriphenylene)$_2$, a Semiconducting Metal-Organic Graphene Analogue. *J. Am. Chem. Soc.* **136**, 8859–8862 (2014).

20. Huang, X. *et al.* A two-dimensional π–d conjugated coordination polymer with extremely high electrical conductivity and ambipolar transport behaviour. *Nat. Commun..* **6**, 7408 (2015).

21. Maeda, H., Sakamoto, R. & Nishihara, H. Coordination Programming of Two-Dimensional Metal Complex Frameworks. *Langmuir* **32**, 2527–2538 (2016).

22. Dou, J.-H. *et al.* Signature of Metallic Behaviour in the Metal-Organic Frameworks M_3(hexaiminobenzene)$_2$ (M = Ni, Cu). *J. Am. Chem. Soc.* DOI: 10.1021/jacs.7b07234.

23. Darago, L. E., Aubrey, M. L., Yu, C. J., Gonzalez, M. I. & Long, J. R. Electronic Conductivity, Ferrimagnetic Ordering, and Reductive Insertion Mediated by Organic Mixed-Valence in a Ferric Semiquinoid Metal–Organic Framework. *J. Am. Chem. Soc.* **137**, 15703–15711 (2015).

24. DeGayner, J. A., Jeon, I.-R., Sun, L., Dincǎ, M. & Harris, T. D. 2D Conductive Iron-Quinoid Magnets Ordering up to T_c = 105 via Heterogeneous Redox Chemistry. *J. Am. Chem. Soc.* **139**, 4175–4184 (2017).

25. Jørgensen, C. K. Differences between the four halide ligands, and discussion remarks on trigonal-bipyramidal complexes, on oxidation states, and on diagonal elements of one-electron energy. *Coord. Chem. Rev.* **1**, 164–178 (1966).

26. Chirik, P. J. & Wieghardt, K. Radical Ligands Confer Nobility on Base-Metal Catalysts. *Science* **327**, 794–795 (2010).

27. Groom, C. R., Bruno, I. J., Lightfoot, M. P. & Ward, S. C. The Cambridge Structural Database. *Acta Cryst. B* **72**, 171–179 (2016).

28. McDowell, C. A., Paulus, K. F. & Rowlands, J. R. Electron-spin Resonance Spectra of Some Diazine Radical Anions. *Proc. Roy. Soc.*, 60–61 (1962).

29. Zhang, X. *et al.* Stabilizing and color tuning pyrazine radicals by coordination for photochromism. *Chem. Commun.* **52**, 7947–7949 (2016).

30. Dunne, T. G. & Hurst, J. K. Kinetic and Thermodynamic Properties of Chromium(III) Complexes Containing Pyrazine Radical Ligands. *Inorg. Chem.* **19**, 1152–1157 (1980).

31. Swartz, J. & Anson, F. C. Electrochemistry of the Intensely Green Complexes Formed by the Reaction of Cr^{2+} with Pyrazine ("Pyrazine Green"), Pyrazinecarboxamide, and Pyrazinecarboxylic Acid. *Inorg. Chem.* **20**, 2250–2257 (1981).

32. Cotton, F. A. *et al.* Experimental and theoretical study of a paradigm Jahn-Teller molecule, all-*trans*-$CrCl_2(H_2O)_2$(pyridine)$_2$, and the related *trans*-$CrCl_2$(pyridine)$_4$·acetone. *Inorg. Chim. Acta* **235**, 21–28 (1995).

29. Cotton, F. A., Favello, L. R., Murillo, C. & Quesada, J. F. A Completely Suppressed Jahn-Teller Effect in the Structure of Hexaaquachromium(II) Hexafluorosilicate. *J. Solid State. Chem.* **96**, 192–198 (1992).

34. Scarborough, C. C. *et al.* Scrutinizing Low-Spin Cr(II) Complexes. *Inorg. Chem.* **51**, 6969–6982 (2012).

35. Glaser, T., Hedman, B., Hodgson, K. O. & Solomon, E. I. Ligand K-edge X-ray Absorption Spectroscopy: A Direct Probe of Ligand-Metal Covalency. *Acc. Chem. Res.* **33**, 859–868 (2000).

36. Miyazaki, A. *et al.* Crystal Structure and Physical Properties of Conducting Molecular Antiferromagnets with a Halogen-Substituted Donor: (EDO-TTFBr$_2$)$_2$FeX$_4$ (X = Cl, Br). *Inorg. Chem.* **46**, 3353–3366 (2007).

37. Solovyev, I. V., Dederichs, P. H. & Mertig, I. Origin of orbital magnetization and magnetocrystalline anisotropy in *TX* ordered alloys (where *T* = Fe, Co and *X* = Pd, Pt). *Phys. Rev. B* **52**, 13419–13428 (1995).

38. Kawamura, N. et al. Multielectron excitations probed by helicity-modulation XMCD a *K*-edge in 3*d* transition metal compounds. *J. Synchrotron Rad.* **8**, 410–412 (2001).

39. Bredas, J. L. & Street, G. B. Polarons, bipolarons, and solitons in conducting polymers. *Acc. Chem. Res.* **18**, 309–315 (1985).

40. Benoit, C., Bernard, O., Palpacuer, M., Rolland, M. & Abadie, M. J. M. Infrared transmission of heavily doped polyacetylene. *J. Phys. France* **44**, 1307–1316 (1983).

41. Jérome, D. Organic Conductors: From Charge Density Wave TTF-TCNQ to Superconducting (TMTSF)$_2$PF$_6$. *Chem. Rev.* **104**, 5565–5591.

42. Roth, S. & Carroll, D. One-dimensional Metals: Conjugated Polymers, Organic Crystals, Carbon Nanotubes and Graphene. John Wiley & Sons, 2015.

43. Li, W., Sun, L., Qi, J., Jarillo-Herrero, P., Dinca, M. & Li. J. High temperature ferromagnetism in π-conjugated two-dimensional metal-organic frameworks. *Chem. Sci.* **8**, 2859–2867 (2017).

44. Kaim, W. & Schwederski, B. Non-innocent ligands in bioinorganic chemistry – An overview. *Coord. Chem. Rev.* **254**, 1580–1588 (2010).

45. Bourges, P., Casalta, H., Ivanov, A. S. & Petitgrand, D. Superexchange Coupling and Spin Susceptibility Spectral Weight in Undoped Monolayer Cuprates. *Phys. Rev. Lett.* **79**, 4906–4909 (1997).

46. Walters, A. C. *et al.* Effect of covalent bonding on magnetism and the missing neutron intensity in copper oxide compounds. *Nat. Phys.* **5**, 867–872 (2009).

47. Kresse, G. & Furthmuller, J. Efficient iterative schemes for *ab initio* total-energy calculations using a plane-wave basis set. *Phys. Rev. B* **54**, 11169–11186 (1996).

48. Kresse, G. & Furthmüller, J. Efficiency of *ab-initio* total energy calculations for metals and semiconductors using a plane-wave basis set. *Comput. Mater. Sci.* **6**, 15–50 (1996).

49. Krukau, A. V., Vydrov, O. A., Izmaylov, A. F. & Scuseria, G. E. Influence of the exchange screening parameter on the performance of screened hybrid functionals. *J. Chem. Phys.* **125**, 224106 (2006).

50. Perdew, J. P., Burke, K. & Ernzerhof, M. Generalized Gradient Approximation Made Simple. *Phys. Rev. Lett.* **77**, 3865–3868 (1996).

51. Kresse, G. & Joubert, D. From ultrasoft pseudopotentials to the projector augmented-wave method. *Phys. Rev. B* **59**, 1758–1775 (1999).